THE JOURNAL OF PHYSICAL CHEMISTRY A
A JOURNAL OF THE AMERICAN CHEMICAL SOCIETY

pubs.acs.org/JPCA Article

Unraveling the Solid-State Photoreactivity of Carbonylbis(4,1-Phenylene)dicarbonazidate with Laser Flash Photolysis

Noha Ahmed, Janaka P. K. Kavikarage, DeAnte F. Judkins,† W. Dinindu Mendis,† Rajkumar Merugu,† Jeanette A. Krause, Bruce S. Ault, and Anna D. Gudmundsdottir*

Cite This: J. Phys. Chem. A 2023, 127, 9705−9716 Read Online

ACCESS | Metrics & More | Article Recommendations | Supporting Information

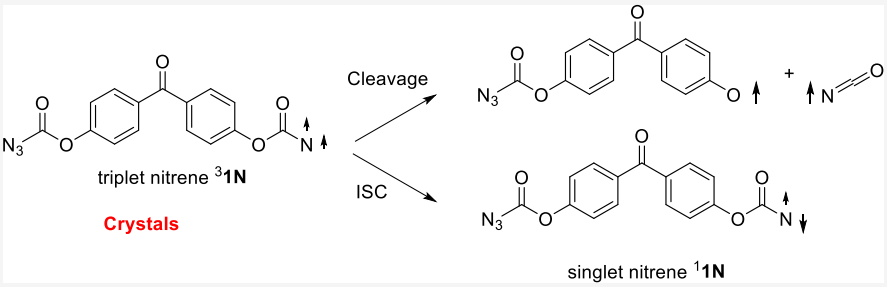

ABSTRACT: Solid-state photoreactions are generally controlled by the rigid and ordered nature of crystals. Herein, the solution and solid-state photoreactivities of carbonylbis(4,1-phenylene)dicarbonazidate (**1**) were investigated to elucidate the solid-state reaction mechanism. Irradiation of **1** in methanol yielded primarily the corresponding amine, whereas irradiation in the solid state gave a mixture of photoproducts. Laser flash photolysis in methanol showed the formation of the triplet ketone (T_K) of **1** ($\tau \sim 99$ ns), which decayed to triplet nitrene ^{3}**1N** ($\tau \sim 464$ ns), as assigned by comparison to its calculated spectrum. Laser flash photolysis of a nanocrystalline suspension and diffuse reflectance laser flash photolysis also revealed the formation of T_K of **1** ($\tau \sim 106$ ns) and ^{3}**1N** ($\tau \sim 806$ ns). Electron spin resonance spectroscopy and phosphorescence measurements further verified the formation of ^{3}**1N** and the T_K of **1**, respectively. In methanol, ^{3}**1N** decays by H atom abstraction. However, in the solid state, ^{3}**1N** is sufficiently long lived to thermally populate its singlet configuration (^{1}**1N**). Insertion of ^{1}**1N** into the phenyl ring to produce oxazolone competes with ^{3}**1N** cleavage to form a radical pair. Notably, **1** did not exhibit photodynamic behavior, likely because the photoreaction occurs only on the crystal surfaces.

1. INTRODUCTION

Due to the rigid and ordered nature of crystals, photoreactions in crystals are typically more selective than their counterparts in solution. Because the reactants are held in fixed positions within the crystal lattice, only reactions that require minimal movement can occur. Reactions that are selective due to the confinement of crystalline reactants are referred to as topochemically allowed reactions.[1] Cohen expanded this concept to define the crystal lattice surrounding a reagent as a reaction cavity, namely, the available space for these molecules to reposition themselves within the crystal lattice without causing major distortions to disrupt the lattice. The crystal lattice thus provides a unique spatial arrangement that controls the selectivity of solid-state reactions.[2−4] The selectivity of solid-state photoreactions is attractive for synthetic applications,[5,6] and this concept has been exploited for the selective formation of some natural products.[7−9] Furthermore, solid-state photoreactions are both environmentally friendly and sustainable because they do not require solvents and can be driven by sunlight or energy-efficient light-emitting diodes.[7,10] However, there are several reactions that exhibit selectivity in the solid state lower than that in solution. Although these reactions are generally not synthetically useful, they can provide insight into how the crystal lattice impedes some reactions but facilitates others.[11−13]

Until recently, advances in solid-state photochemistry were limited by a lack of suitable techniques for mechanistic analysis. The reflectance of many bulk solids hinders the use of standard transient absorption spectroscopy or laser flash photolysis to detect the excited states and reactive intermediates formed within crystals, which is necessary to elucidate solid-state reaction mechanisms. Thus, the understanding of solid-state reactions has typically relied on structure−reactivity correlations, such as those obtained by Schmidt in the 1960s for *trans*-cinnamic acids.[1] Recent work

Received: July 19, 2023
Revised: October 25, 2023
Accepted: October 26, 2023
Published: November 8, 2023

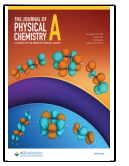

by Garcia-Garibay and collaborators[14−16] has provided an innovative solution by adapting a reprecipitation method first described by Kasai et al.[17] to suspend nanocrystals in a solvent. This approach allows for time-resolved spectroscopic analyses because the average size of the crystals is smaller than the irradiation wavelength.[18,19]

An emerging aspect of solid-state photochemistry is the physical response of crystals to the buildup of photoproducts within the crystal lattice, referred to as the photodynamic behavior of crystals.[20,21] Owing to changes induced by product formation upon irradiation, crystals can convert light into mechanical movement including jumping, twisting, or cracking.

In this work, we investigated the photoreactivity of carbonylbis(4,1-phenylene)dicarbonazidate (**1**), which has a benzophenone chromophore that acts as a built-in triplet sensitizer. Upon irradiation, the benzophenone chromophore absorbs light to form the triplet excited state of benzophenone, which transfers its energy to the azido chromophore, thereby bypassing the direct excitation of the azido chromophore and the direct formation of the corresponding singlet nitrene.[22] We employed laser flash photolysis of **1** in solution and the solid state by using nanosuspensions and diffuse reflectance to understand how the crystal lattice affects the reaction mechanism.

2. METHODS

2.1. Synthesis of the Starting Material. *2.1.1. Synthesis of Carbonylbis(4,1-Phenylene)dicarbonazidate (1).* A solution of triphosgene (1.2 g, 4.2 mmol) in dry methyltetrahydrofuran (mTHF, 50 mL) was added dropwise over 30 min to a round-bottom flask containing 4,4′-dihydroxybenzophenone (1.5 g, 7.0 mmol) and *N*,*N*-dimethylaniline (1.8 mL, 14 mmol) in dry mTHF (50 mL) at −10 °C. The reaction mixture was slowly brought to room temperature while being stirred for 3 h. After adding sodium azide (0.65 g, 10 mmol), the resulting solution was stirred overnight, extracted with diethyl ether (3 × 50 mL), and dried over magnesium sulfate. The solvent was removed under reduced pressure and the product was purified by washing with petroleum ether to yield a white solid (800 mg, 2.3 mmol, 33% yield). Azide **1** was characterized by using infrared (IR), ^{1}H nuclear magnetic resonance (NMR), and ^{13}C NMR spectroscopy and high-resolution mass spectrometry (HRMS).

mp 122−123 °C. IR (solid): 2199, 2161, 1739, 1648, 1597, 1501, 1411, 1246, 1197, 1152, 1011, 930, 749 cm^{-1}. ^{1}H NMR (400 MHz, CD_3CN): δ 7.86 (d, J = 8.4 Hz, 1H), 7.39 (d, J = 8.3 Hz, 1H). ^{13}C NMR (101 MHz, CD_3CN): δ 193.4, 155.6, 153.4, 135.2, 131.3, 120.9. HRMS (m/z): $[M + H]^+$ calcd for $C_{15}H_8O_5N_6$, 353.0634; found, 353.0616; $[M + Na]^+$ calcd for $C_{15}H_8O_5N_6$, 375.0454; found, 375.0456.

2.2. Photolysis of 1. *2.2.1. Photolysis of 1 in Methanol.* A round-bottom Pyrex flask containing a solution of **1** (60 mg, 0.17 mmol) in methanol (100 mL) was purged with argon for 15 min, and the stopcock and the vessel were sealed with parafilm. It was irradiated for 2.5 h using a medium-pressure mercury arc lamp housed in a Pyrex cooling jacket. The solvent was evaporated under reduced pressure to yield a solid residue (∼59 mg). The sample was redissolved in methanol, and acetone trituration of the reaction mixture resulted in the precipitation of carbonylbis(4,1-phenylene)dicarbamate **2** (30 mg, 0.10 mmol, 60% yield). Amine **2** was characterized by using IR, ^{1}H NMR, and ^{13}C NMR spectroscopy and HRMS. mp 168−170 °C. IR (solid): 3421, 3333, 3278, 3187, 1697, 1655, 1593, 1500, 1359, 1298, 1271, 1204, 1154, 1103, 1022, 970, 626, 503 cm^{-1}. ^{1}H NMR (400 MHz, DMSO-d_6): δ 7.78 (d, J = 8.2 Hz, 2H), 7.39 (s, 1H), 7.30 (d, J = 8.2 Hz, 2H), 7.15 (s, 1H). ^{13}C NMR (101 MHz, DMSO-d_6): δ 193.7, 154.4, 154.1, 133.5, 131.1, 121.9. HRMS (m/z): $[M + Na]^+$ calcd for $C_{15}H_{12}O_5N_2$, 323.0644; found, 323.0643.

2.2.2. Solid-State Photolysis of 1. Azide **1** (147 mg, 0.4 mmol) was placed between two Pyrex watch glasses and irradiated with a medium-pressure mercury arc lamp for 71 h. The reaction mixture was dissolved in acetonitrile-d_3 and analyzed by using ^{1}H NMR spectroscopy. The reaction mixture was purified on a silica column and eluted with hexane/ethyl acetate (80/20) to obtain **1** as the major fraction (90.7 mg, 0.26 mmol, 62% yield) along with four new fractions.

Using IR, ^{1}H NMR, and ^{13}C NMR spectroscopy and HRMS, the major photoproduct was identified as 4-(2-oxo-2,3-dihydrobenzo[*d*]oxazole-5-carbonyl)phenyl carbonazidate (**3**; 19.5 mg, 0.0601 mmol, 13.3% yield). IR: 3189, 2924, 2163, 1736, 1650, 1598, 1464, 1359, 1197, 1152, 1095, 926, 753 cm^{-1}. ^{1}H NMR (400 MHz, CD_3CN): δ 9.31 (s, 1H), 7.87 (d, J = 8.5 Hz, 2H), 7.58 (dd, J = 8.3, 1.7 Hz, 1H), 7.53 (d, J = 1.7 Hz, 1H), 7.41 (d, J = 8.5 Hz, 2H), 7.33 (d, J = 8.3 Hz, 1H). ^{13}C NMR (101 MHz, CD_3CN): δ 194.9, 157.0, 155.0, 154.5, 148.0, 136.9, 134.2, 132.6, 130.1, 125.2, 122.3, 112.0, 110.2. HRMS (m/z): $[M + H]^+$ calcd for $C_{15}H_8N_4O_5$, 325.0573; found, 325.0576.

The second fraction was mainly 4-(4-hydroxybenzoyl)-phenyl carbonazidate (**4**; 13.1 mg, 0.046 mmol, 8.92% yield). IR: 3217, 2162, 1770, 1741, 1649, 1598, 1509, 1437, 1311, 1274, 1148, 1013, 928 cm^{-1}. ^{1}H NMR (400 MHz, CD_3CN): δ 7.87−7.79 (m, 2H), 7.79−7.65 (m, 2H), 7.71 (s, 1H), 7.43−7.34 (m, 2H), 6.99−6.89 (m, 2H). ^{13}C NMR (101 MHz, CD_3CN): δ 193.8, 161.8, 156.3, 152.3, 138.2, 132.5, 131.0, 128.1, 122.1, 115.2. HRMS (m/z): $[M + H]^+$ calcd for $C_{14}H_9N_3O_4$, 284.0666; found, 284.0669.

The third fraction was identified as 5-(4-hydroxybenzoyl)-benzo[*d*]oxazol-2(3*H*)-one (**5**; 7.4 mg, 0.030 mmol, 5.8% yield). IR: 3311, 1756, 1632, 1584, 1602, 1453, 1443, 1312, 1278, 1177, 1095, 931, 845, 766 cm^{-1}. ^{1}H NMR (400 MHz, CD_3CN): δ 8.26 (s, 2H), 7.76−7.65 (m, 2H), 7.57−7.44 (m, 2H), 7.31 (d, J = 8.3 Hz, 1H), 6.99−6.89 (m, 2H). ^{13}C NMR (101 MHz, CD_3CN): δ 194.1, 161.1, 154.9, 148.0, 136.7, 133.0, 130.2, 129.4, 124.9, 114.4, 110.6, 109.0. HRMS (m/z): $[M + H]^+$ calcd for $C_{14}H_9NO_4$, 256.0610; found, 256.0611.

The last fraction contained bis(4-hydroxyphenyl)methanone (**6**; 7.5 mg, 0.035 mmol, 5.1% yield). The obtained IR and NMR spectra were consistent with those reported previously.[23] IR: 3330, 3133, 1626, 1567, 1506, 1444, 1240, 1151, 851 cm^{-1}. ^{1}H NMR (400 MHz, CD_3CN): δ 7.77−7.65 (m, 2H), 7.61 (s, 1H), 6.99−6.89 (m, 2H). ^{13}C NMR (101 MHz, CD_3CN): δ 194.4, 161.2, 132.8, 130.7, 115.4. HRMS (m/z): calcd for $C_{13}H_{10}O_3$, 214.0630; found, 214.0619.

2.2.3. Photolysis of 1 in Nanosuspension. A nanocrystal suspension of **1** was prepared by dissolving **1** (30 mg) in acetone (203 mL) and adding 250 mL of water.[26] The size of the nanocrystals was measured by using dynamic light scattering (DLS, see Supporting Information), which showed 77% of the nanocrystals were less than 486 nm. The nanosuspension was irradiated for 20 min, and ^{1}H NMR spectra of the reaction mixture showed the formation of **3** and **4** in the ratio of ∼1:1.

https://doi.org/10.1021/acs.jpca.3c04867
J. Phys. Chem. A 2023, 127, 9705−9716

Scheme 1. Photoproducts Formed by Irradiating 1 in Methanol and the Solid State

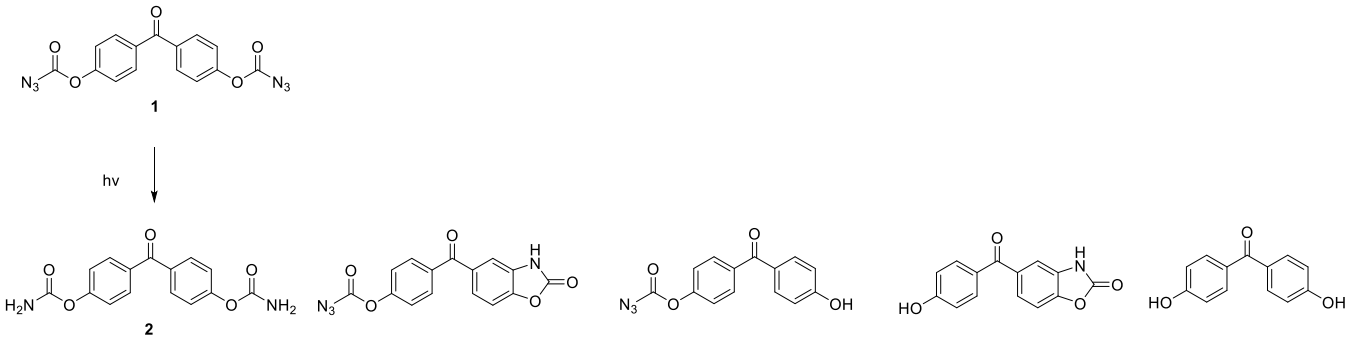

Product	2	3	4	5	6
Methanol	Major				
Solid state (%)		13	9	6	5

2.3. Laser Flash Photolysis. Laser flash photolysis was performed using a commercially available laser flash photolysis system (LP980, Edinburgh Instruments, Inc.) with 266 nm laser irradiation (Nd/YAG, Surelite II, Continuum, Inc.).[24,25] All spectra and kinetic traces were obtained at room temperature in a 1 cm flow cell at a flow rate of 1 mL/min. A stock solution was prepared by using spectroscopic-grade methanol or acetonitrile. The absorption of each sample was between 0.2 and 0.8 at 266 nm.

For nanocrystal suspensions,[26] a stock solution was prepared by dissolving 1−4 mg of **1** in 2−3 mL of acetone. Approximately 0.4−0.6 mL of this stock solution was added over 4 min to 500 mL of deionized water containing 0.4×10^{-3} M hexadecyltrimethylammonium bromide (CTAB) under sonication. A clear solution was obtained, and the size of the crystals was measured by using DLS. The sample was suitable for analysis by laser flash photolysis as 80% of the crystals had sizes of 429 nm and less (see the Supporting Information). Argon- and oxygen-saturated solutions were prepared by purging with argon or oxygen for 20−25 min.

Diffused reflectance laser flash photolysis was carried out with the same laser flash photolysis apparatus as described above but with a sample holder for the solid material (Edinburgh Instrument, Inc.). An excimer laser (λ = 308 nm)[24] was used to obtain the transient absorption. For argon- and oxygen-equilibrated measurements, 100 mg of solid was placed in a 3×7 mm^2 cuvette for 30 min. For air-equilibrated measurements, 30−40 mg of the crystals was ground into a fine powder and loaded directly onto the sample holder. Transient absorption spectra were measured by using an I-CCD detector, and kinetic traces were measured with a PMT detector.

2.4. Phosphorescence. The phosphorescence of **1** was measured in a glassy mTHF matrix or in the solid state using a phosphorimeter, as described previously.[27] The phosphorescence of **1** in mTHF (33 mM) was measured at 77 K with 270 nm excitation. The phosphorescence of **1** in the solid state with 270 nm excitation was obtained by placing finely crushed crystals of **1** in a quartz NMR tube and recording the emission at 77 K.

2.5. EPR Spectroscopy. Frozen X-band EPR spectra were recorded on a Bruker EMX EPR spectrometer equipped with an ER-4116DM dual-mode resonator, with the temperature maintained at 4.5 K by an Oxford ESR900 flow cryostat. Azide **1** was dissolved in mTHF forming a 2.0 mM solution. The solution was placed in a Wilmad Low Pressure/Vacuum Suprasil EPR tube, filling the tube with ∼5 cm of sample. The sample was degassed by using the freeze−pump−thaw method until bubble formation ceased. In the EPR instrument, the solution temperature was lowered to 5 K forming a glassy matrix. The system was calibrated by placing the monitoring frequency at 9.390620 GHz. The sample was irradiated using a 254 nm UV pen for different time intervals showing signal formation.

2.6. Argon Matrix Trapping of the Gaseous Products from Solid-State Irradiation of 1. The setup for cryogenic matrix isolation has been described previously.[28] Crystals of **1** (∼20 mg) were placed in a quartz tube connected to an argon deposition line outside of the cold cell. The quartz glass segment was irradiated using a 254 nm UV pen for 21 h while argon flowed over the crystals. The argon flow containing volatile photoproduct(s) was condensed on a 14 K cold window and monitored by IR spectroscopy at different time intervals.

2.7. Calculations. The geometries of **1**, T_1 of **1**, ^{3}**1N**, and ^{1}**1N** were optimized using the B3LYP level theory with a 6-31+G(d) basis set using Gaussian16 software.[29−31] Single-point time-dependent density functional theory (TD-DFT) calculations [B3LYP/6-31+G(d)] were used to estimate the vertical energies of the first singlet state (S_1) and T_1 of **1**. In addition, the absorption spectra of T_1 of **1** and ^{3}**1N** were calculated using TD-DFT calculations.[31,32] All transition states were confirmed by the analysis of one imaginary vibrational frequency, as determined by the second derivative of the energy with respect to the optimized internal coordinates. Intrinsic reaction coordinate calculations were used to verify that the transition state correlates to the appropriate reagent and product.[33,34]

2.8. Powder Diffraction Experiment. Finely ground powdered samples were analyzed at room temperature using Cu Kα radiation (3−100 deg in θ−2θ, 2 deg/min, 0.01 deg step width, reflection mode) on a Rigaku Mini-Flex 6G diffractometer. Diffractograms collected on **1** were prior to irradiation, after irradiation for ∼1 day, and after irradiation for ∼2.5 days. Samples were irradiated using a mercury arc lamp through a Pyrex filter.

3. RESULTS AND DISCUSSION

3.1. Product Studies. *3.1.1. Photolysis of 1 in Methanol.* Irradiation of **1** in argon-saturated methanol yielded **2** as the major product (Scheme 1). We propose that the triplet

https://doi.org/10.1021/acs.jpca.3c04867
J. Phys. Chem. A 2023, 127, 9705−9716

Scheme 2. Proposed Mechanism for the Formation of 2 via the Photolysis of 1 in Methanol

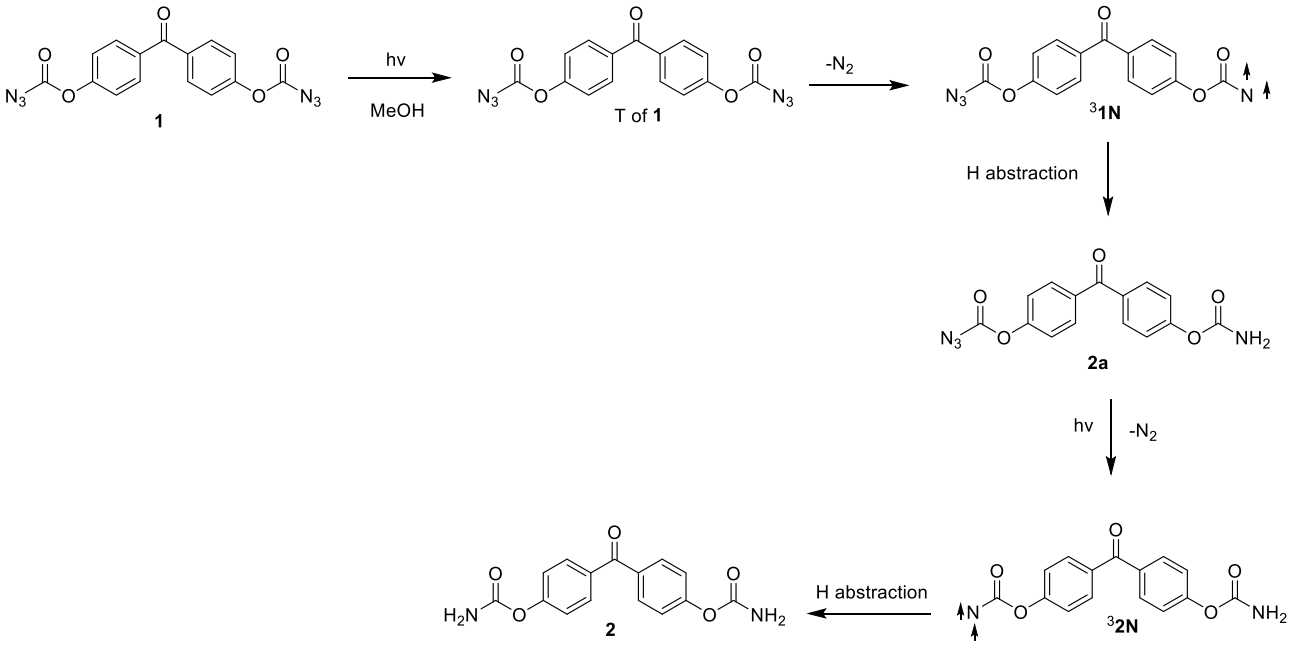

Scheme 3. Proposed Mechanism for the Solid State Photoreactivity of 1

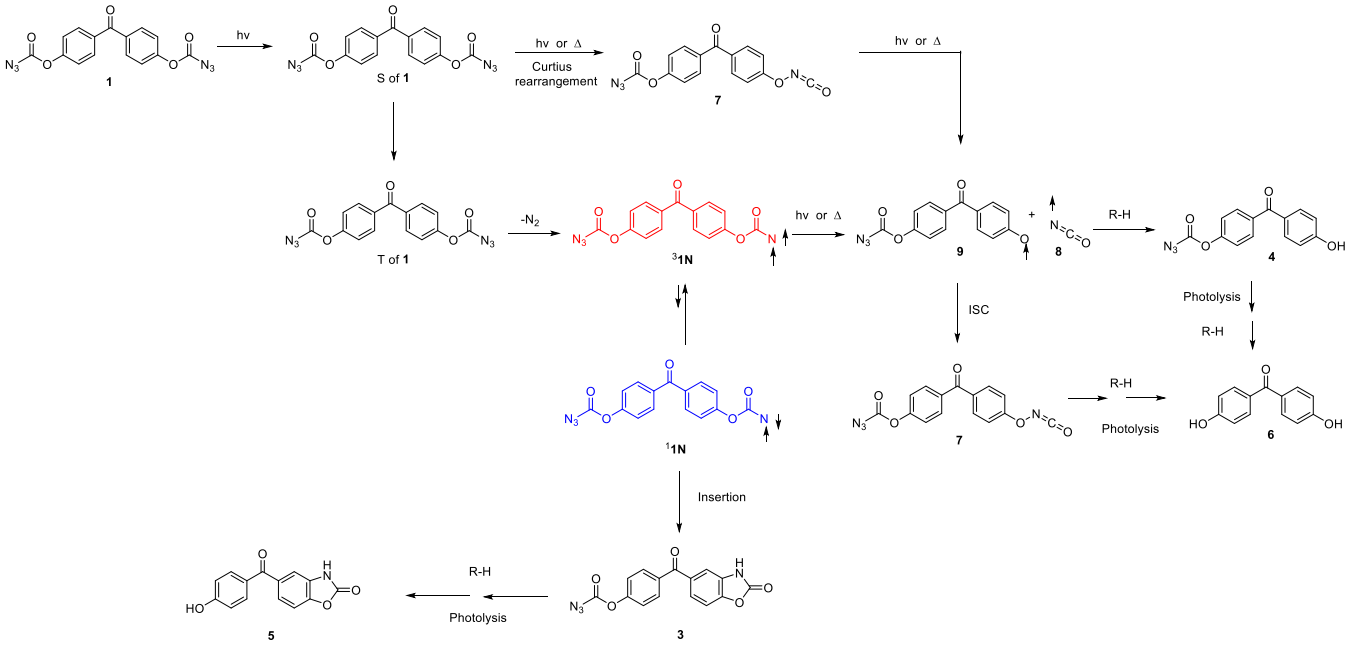

configuration of the ketone (T_K) of **1** is formed upon excitation. The energy of T_K of **1** is subsequently transferred to the azido moiety to give the triplet state of the azide chromophore (T_A), which releases a nitrogen molecule to yield triplet nitrene ^{3}**1N**. Nitrene ^{3}**1N** is presumed to decay by abstracting an H atom from the methanol solvent to form radical 2H that abstracts another H atom from the solvent to form amide **2a**. Absorption of a second photon produces nitrene ^{3}**2N**, which also abstracts an H atom to yield **2** (Scheme 2). As with other ester azides with either built-in triplet sensitizers or bimolecular sensitization,[22,35,36] excitation in solvents with abstractable H atoms mainly yields the corresponding amines.

3.1.2. Solid-State Photolysis of 1. The photoreaction of **1** in the solid state is less selective than that in methanol. Upon irradiation, the crystals of **1** turned yellow (Figure S11). However, high conversion could not be achieved because the reaction occurred only on the crystal surfaces. ^{1}H NMR analysis of the solid-state reaction mixture dissolved in acetonitrile-*d*3 revealed that the major product was oxazolone **3**, which formed along with products **4**, **5**, and **6** in a ratio of 2.6:1.2:1.8:1 (Scheme 1). Irradiation of **1** (20 min) in a nanosuspension showed the formation of photoproducts **3** and **4** in the ratio of ∼1:1. Because the same initial photoproducts are formed in nanosuspensions as in bulk crystals, we did not continue the irradiation further. It should be noted that irradiating **1** in nanosuspensions or bulk crystals does not yield

https://doi.org/10.1021/acs.jpca.3c04867
J. Phys. Chem. A 2023, 127, 9705−9716

amine **2**. Irradiation of **1** yields nitrene ^{3}**1N** via the energy transfer from the T_K of **1**. Owing to the absence of easily abstractable H atoms in **1**, ^{3}**1N** cannot decay by an H atom abstraction. Instead, nitrene ^{3}**1N** is anticipated to be in equilibrium with its singlet configuration ^{1}**1N**, which can insert into the benzene ring to yield **3** (Scheme 3).[36] In addition, nitrene ^{1}**1N** can form isocyanate **7** via the Curtius rearrangement in a concerted manner, thermally or photochemically.[36−38] However, it is also possible that nitrene ^{3}**1N** cleaves to form the phenoxy and isocyanate radical pair **8** and **9**, which can combine to form **7**. The radical pair **8** and **9** can potentially also abstract H atoms to form phenol derivatives **4**, **5**, and **6** and isocyanic acid, although it is not clear what the actual source of H atoms is in the solid state, as **1** does not have easily abstractable H atoms. Thus, the phenol moiety in photoproducts **4**, **5**, and **6** is expected to be formed via H atom abstraction by a phenoxy radical derivative, whereas the oxazolone chromophore originates from ^{3}**1N** intersystem crossing to ^{1}**1N**.

3.1.3. Isocyanic Acid Trapping in an Argon Matrix. To support the notion that isocyanic radical **8** is formed in the solid state and to determine whether **8** abstracts an H atom to form isocyanic acid, the gaseous products obtained upon irradiation of a crystalline sample of **1** were trapped in an argon matrix and analyzed using IR spectroscopy. Product bands were observed at 2261, 2260, 770, and 574 cm^{-1} (Figure 1). The shoulder at 2261 cm^{-1} is likely due to the site splitting of the band at 2260 cm^{-1}. The intensities of these bands increased as a function of irradiation time (Figure 1). These bands were assigned to isocyanic acid based on comparison with the reported IR spectrum in argon matrices, which has bands at 2260, 770, and 573 cm^{-1}.[39,40] Additionally, the calculated [B3LYP/6-31+G(d)] and scaled (0.9613)[41] spectrum of isocyanic acid has significant bands at 2242, 725, and 544 cm^{-1}, which further supports this assignment.

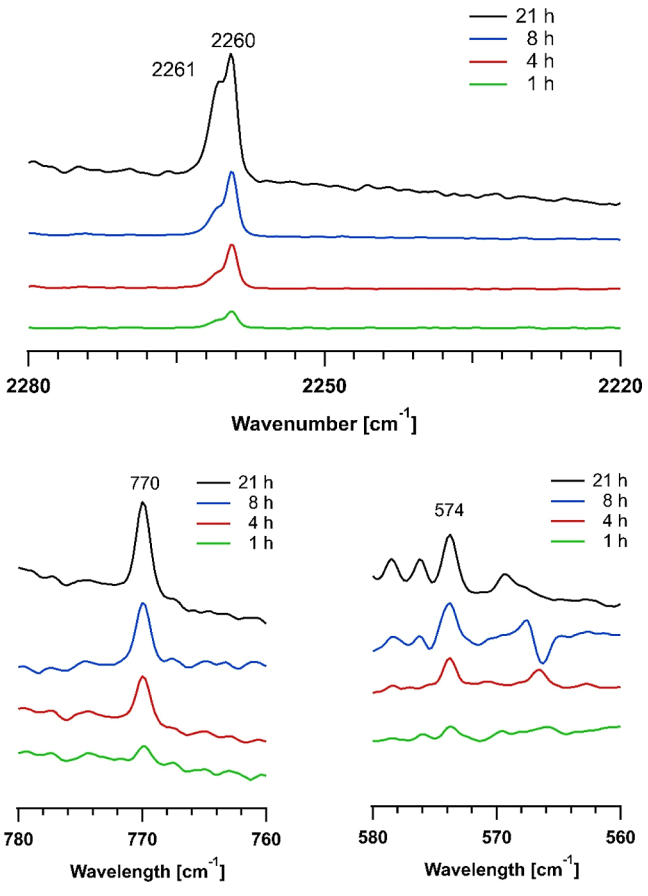

Figure 1. IR spectra of isocyanic acid trapped in argon matrices as a function of the irradiation time of **1**.

Thus, we theorize that irradiation of solid **1** forms nitrene ^{3}**1N** (Scheme 4), which is cleaved either thermally or photochemically to give the radical pair **8** and **9**. The radical pair can form **7** or abstract an H-atom to yield isocyanic acid and **4**. Isocyanide **7** and **4** are likely not volatile enough to be deposited in the argon matrix. While the argon matrix experiments were conducted under a high vacuum of 10^{-7} torr, some residual air remained in the system. Water is a particularly "sticky" molecule, adsorbing onto metal and quartz surfaces. Consequently, some residual water is present at all times and is seen at impurity levels in nearly all argon matrix spectra (see the Supporting Information). Therefore, it is theorized that the H atom in isocyanic acid originates from atmospheric moisture on the crystal surface.

3.2. Laser Flash Photolysis of 1. *3.2.1. Laser Flash Photolysis of 1 in Solution.* To verify that the photoreactivity of **1** occurs on the triplet surface, we performed laser flash photolysis in methanol and acetonitrile. Laser flash photolysis of **1** in argon-saturated methanol and acetonitrile (Figures 2 and 3, respectively) resulted in two absorption bands with λ_{max} values at ∼330 and ∼540 nm. As the transient absorption decayed in methanol, the band at 540 nm shifted toward 560 nm. We assigned the transient with λ_{max} at 330 and 540 nm to the T_K of **1** based on its TD-DFT-calculated spectrum, which placed the most intense electron transitions at 326 (f = 0.1138), 336 (f = 0.2953), 533 (f = 0.0098), 565 (f = 0.0266), and 587 nm (f = 0.2528) (Figure 2B). This assignment was also supported by comparison with the triplet excited state of benzophenone, which yields a similar transient absorption spectrum.[42] The transient with λ_{max} at 560 nm in methanol was assigned to ^{3}**1N** based on its TD-DFT-calculated spectrum, which exhibited several weak electronic transitions at 522 nm (f = 0.0011), 552 nm (f = 0.0013), 605 nm (f = 0.0113), and 647 nm (f = 0.0092) (Figure 2C).

The kinetic traces further confirmed these assignments. In argon-saturated acetonitrile, the decay was best fitted as a monoexponential function, resulting in a lifetime (τ_4) of 337 ns ($k_4 \sim 2.97 \times 10^6$ s^{-1}). In air- and oxygen-saturated acetonitrile, the lifetimes became shorter or (τ_5) 137 and (τ_6) 60 ns, respectively (Figure 3B). Because the estimated oxygen concentration in oxygen-saturated and air-saturated acetonitrile is 9.1 and 1.9 mM, respectively,[43] it can be inferred that the rate constant for oxygen quenching is between 1.8 and 3.8 $\times 10^9$ M^{-1} s^{-1}. This finding provides additional evidence for the transient being the T_K of **1** as it is expected that oxygen reacts less efficiently with ^{3}**1N**.[44]

In contrast, the decay in methanol at 540 nm could be fitted as a biexponential function (Figure 2D), resulting in decay rate constants (k_1) of 1.01 $\times 10^7$ s^{-1} ($\tau_1 \sim 99$ ns) and (k_2) of 2.13 $\times 10^6$ s^{-1} ($\tau_2 \sim 464$ ns). We assigned the faster rate constant (k_1) to the T_K of **1**, which decays to form nitrene ^{3}**1N**, whereas the slower rate constant (k_2) was assigned to the decay of ^{3}**1N**. As expected, the decay became faster in oxygen-saturated methanol due to oxygen quenching the T_K of **1**, and it was best fitted as a monoexponential function with a rate constant (k_3) of 1.91 $\times 10^8$ s^{-1} (τ_3 = 52 ns). Because the T_K of **1** is sufficiently short-lived in methanol, we can detect nitrene ^{3}**1N**

https://doi.org/10.1021/acs.jpca.3c04867
J. Phys. Chem. A 2023, 127, 9705−9716

Scheme 4. Potential Mechanism for the Formation of Isocyanic Acid via the Photolysis of Solid 1 under an Argon Atmosphere

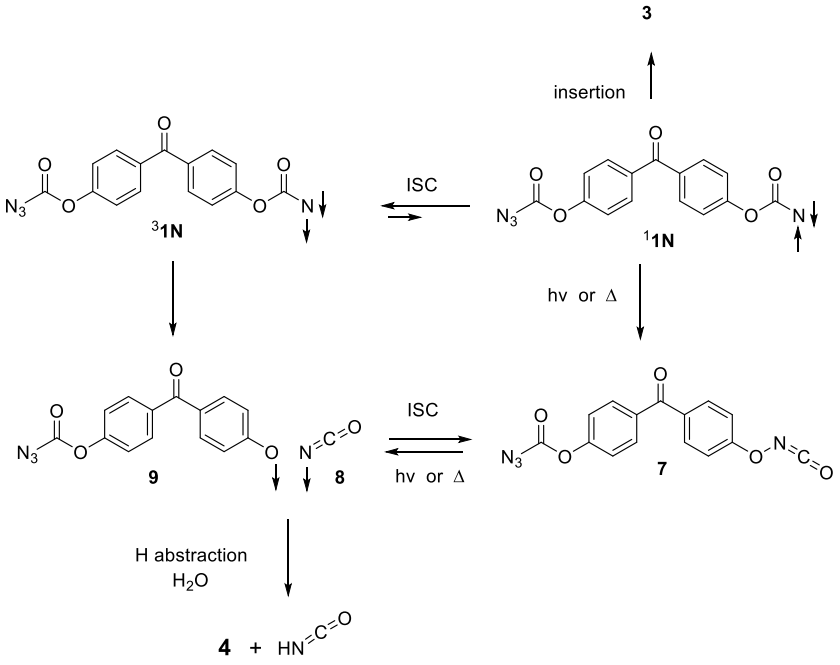

directly. However, in acetonitrile, the T_K of **1** masks the absorption of ^{3}**1N**, thereby preventing the determination of its lifetime.

3.2.2. Laser Flash Photolysis of Aqueous Nanocrystalline Suspension. The transient absorption spectra obtained by laser flash photolysis of **1** in a nanocrystalline suspension were similar to those obtained in solution, but the intensity was much weaker (Figure 4). The kinetic decay at 540 nm was best fitted as a biexponential function, resulting in rate constants of 1.25×10^6 s^{-1} ($\tau \sim 806$ ns) and 9.53×10^6 s^{-1} ($\tau \sim 105$ ns). Thus, the lifetime of T_K of **1** is similar in the solid state and in methanol, whereas the lifetime of nitrene ^{3}**1N** is slightly longer in the solid state. Thus, we propose that the observed rate constant corresponds to nitrene ^{3}**1N** decaying by intersystem crossing to its singlet configuration (^{1}**1N**) and that the crystal lattice unmasked this slower reaction because the faster H-atom abstraction process was blocked.

3.2.3. Diffuse Reflectance Laser Flash Photolysis. We also investigated the transient absorption obtained by the laser flash photolysis of a solid sample of **1** using diffuse reflectance (Figure 5). The results of these experiments were similar to those obtained for the nanocrystalline suspension, although observation of the transient absorption spectra was difficult due to scattering. However, as the lifetimes of T_K of **1** and ^{3}**1N** were the same within experimental error, these results confirm that the reactivities in nanocrystals and bulk crystals are similar.

3.3. Phosphorescence. To verify that irradiation of **1** results in the formation of T_K of **1** and that we are bypassing the direct formation of ^{1}**1N**, both in the solid state and solution, we measured its phosphorescence (Figure 6). The phosphorescence of **1** in mTHF and the solid state displayed similar resolved vibrational features as generally observed for ketones with the (n,π^*) configuration.[45] In mTHF, the (0,0) band is located at 417 nm (Figure 6); this corresponds to the T_K of **1** at 69 kcal/mol above S_0 of **1**, whereas the (0,0) band in the solid state is located at 430 nm or at 66 kcal/mol. Thus, the T_K of **1** is better stabilized in the solid state than in mTHF. Thus, the crystal lattice has some effect on the emission but is not significant.[46,47]

3.4. Electron Spin Resonance Spectroscopy. Electron spin resonance (ESR) spectroscopy was used to verify that irradiation of azide **1** results in the formation of nitrene ^{3}**1N**. Upon irradiation of **1** at 254 nm in a mTHF matrix at 5 K, weak ESR signals appeared at 7805 and 8910 G, which grew upon further irradiation (Figure 7). The zero-field splitting (zfs) parameters for ^{3}**1N** were calculated using the X_2 and Y_2 signals of the spectrum according to the Wasserman equations.[48] The calculated zfs parameters for ^{3}**1N** (D/hc = 1.387 cm^{-1} and E/hc = 0.0013 cm^{-1}) were characteristic of ester nitrenes.[35,37,48] For example, Schuster and co-workers reported that the ESR spectrum of 4-acetylbenzoylnitrene has zfs parameters of D/hc = 1.65 cm^{-1} and E/hc = 0.024 cm^{-1}.[35] Wentrup and collaborators demonstrated that there is a linear correlation between the D/hc value and the calculated spin density on the N atom in triplet nitrenes.[49−51] This general relationship held true for nitrene ^{3}**1N**, which has a calculated spin density of 1.8.

3.5. Photodynamic Behavior of 1. We have previously shown that the reactions of crystalline organic azides can result in a large photodynamic response when N_2 gas is released.[52,53] The solid-state photoreaction of **1** was followed by using a digital microscope. Crystals of **1** were grown from an acetone−water mixture; it should be noted that these crystals were small and not suitable for a single crystal X-ray structure analysis. During irradiation with a mercury arc lamp pen, the crystals gradually became opaque (Figure 8) and their surfaces turned yellow (Figure S11). However, the size and shape of the crystals did not change, presumably because the solid-state reaction occurred only on the surface of the crystals, with the product forming a thin layer that prevented further reaction and any photodynamic response leading to product formation. Similarly, irradiation of feather-like crystals grown from methanol with a 254 nm UV pen resulted in the crystals turning yellow but no photodynamic response was observed.

https://doi.org/10.1021/acs.jpca.3c04867
J. Phys. Chem. A 2023, 127, 9705−9716

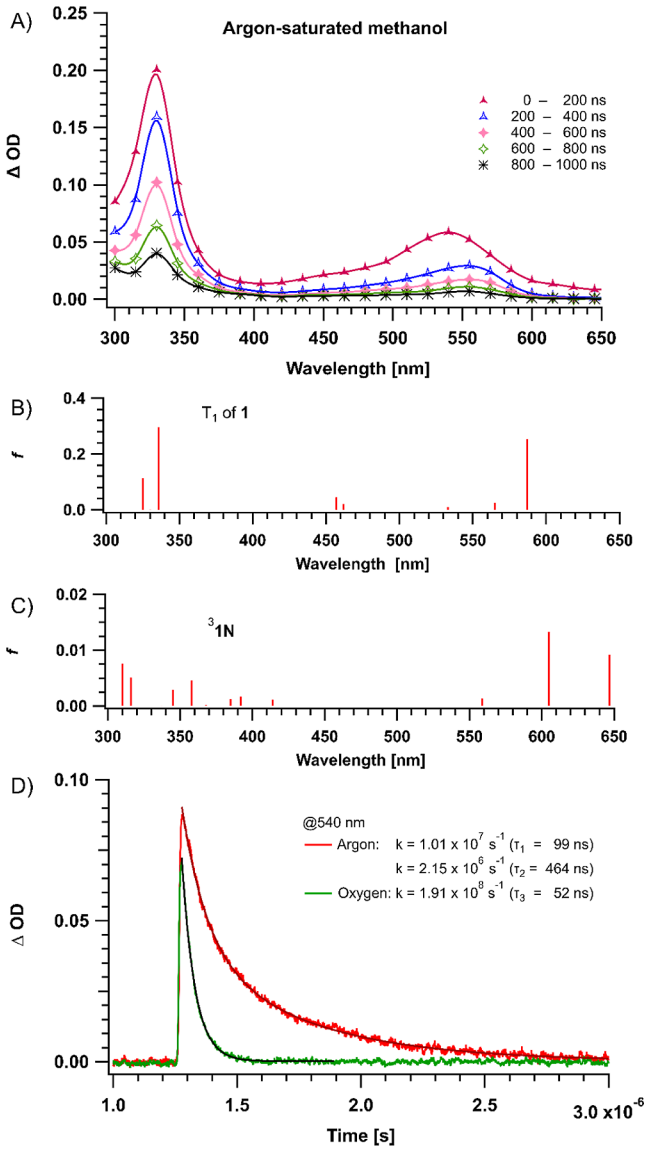

Figure 2. (A) Transient absorption spectra obtained by laser flash photolysis of **1** in argon-saturated methanol. TD-DFT-calculated electronic transitions for (B) T_K of **1** and (C) ^{3}**1N**. (D) Kinetic traces obtained by laser flash photolysis of **1** in argon- (red) and oxygen-saturated (green) methanol at 540 nm. The black traces are the fitting curves for the decays.

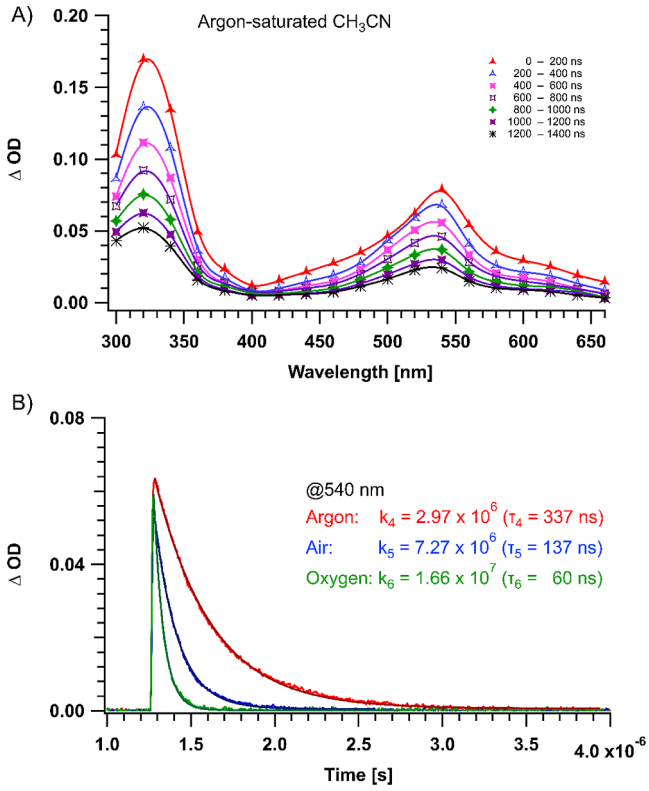

Figure 3. (A) Transient absorption spectra obtained by laser flash photolysis of **1** in argon-saturated acetonitrile. (B) Kinetic traces obtained by laser flash photolysis of **1** in argon-, air-, and oxygen-saturated acetonitrile at 540 nm.

3.6. Powder X-ray Diffraction. Because the crystal of **1** did not diffract sufficiently to determine the crystal structure, we obtained powder diffractograms of **1** before and after irradiation (Figure 9). The diffractograms of the photolyzed samples of **1** do not show significant differences from the nonirradiated sample, thus further supporting that the solid-state reaction of **1** is only taking place on the surface of the crystals.

3.7. Quantum Chemical Calculations. To support the proposed photoreactivity mechanisms shown in Schemes 2 and 3, DFT calculations were performed using Gaussian16[29] at the B3LYP level of theory with the 6-31+G(d) basis set.[30,31] The optimized structures of **1**, T_K of **1**, T_A of **1**, and ^{3}**1N** are shown in Figure 10. TD-DFT calculations placed S_1 and T_1 of **1** at 82 and 69 kcal/mol above S_0, respectively. Two different triplet configurations were optimized for **1**. The configuration located 64 kcal/mol above S_0 of **1** was considered to correspond to a triplet ketone with a (n,π^*) configuration because the spin density calculations placed most of the unpaired electrons on the C═O group [O (0.96) and C (0.40)]. Thus, we assigned this configuration to the T_K of **1** and note that both the calculated energy and the configuration of T_K of **1** correspond to those obtained from the phosphorescence measurements. The other optimized triplet was located 55 kcal/mol above the S_0 of **1** and had a N−N−N angle of 121°. Thus, we assigned this configuration to the triplet azido chromophore (T_A of **1**). Spin density calculations further supported this assignment, as the unpaired electrons were mainly located on the N_α (0.9) and N_γ (0.8) atoms.

For the optimized structure of nitrene ^{3}**1N**, the spin density calculations placed the unpaired electrons on the N atom (1.8). Optimization of ^{1}**1N** using the broken symmetry method revealed that it is located 9 kcal/mol above its triplet configuration. In more detail, the broken symmetry calculations used to optimize the structure of nitrene ^{1}**1N**, which was obtained by using guess = mix as a keyword in Gaussian16, yielded nitrene ^{1}**1N** with a total spin (⟨S2⟩) value of 0.91, which has significant spin contamination from the triplet state. Due to the high degree of spin contamination in the singlet, however, the DFT-calculated energy gap is not considered to be very reliable.[54] The energy gap for a similar oxycarbonyl nitrene has been calculated as 13 kcal/mol using a higher level of theory (CASPT2(12,11)/6-311G**);[37] thus, we assume that the energy gap is comparable for ^{1}**1N** and ^{3}**1N**.

The calculated stationary points on the singlet and triplet surfaces of **1** are shown in Figure 11. Because T_A of **1** has a lower energy than the T_K of **1**, it is anticipated that T_A of **1** is formed through intramolecular triplet sensitization. As the

https://doi.org/10.1021/acs.jpca.3c04867
J. Phys. Chem. A 2023, 127, 9705−9716

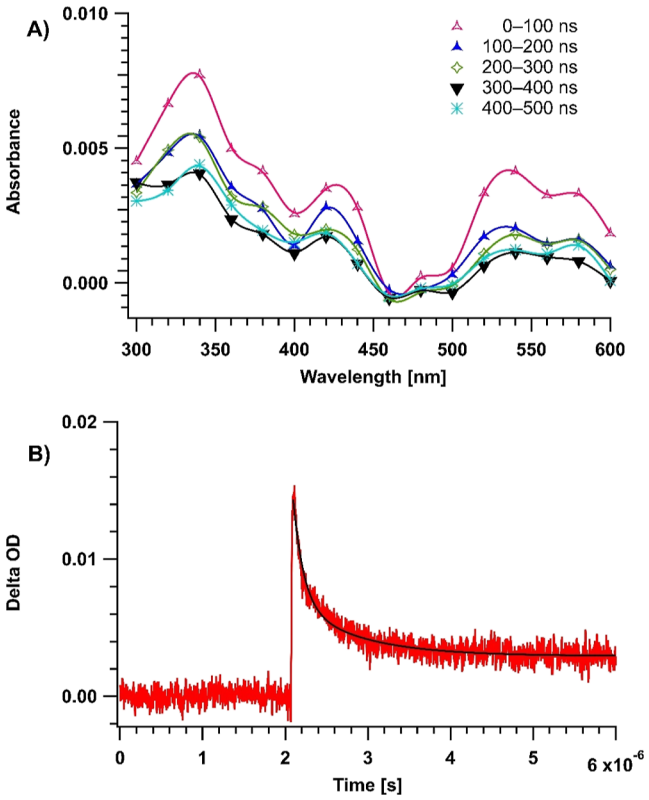

Figure 4. (A) Transient absorption spectra and (B) kinetic trace at 540 nm obtained by laser flash photolysis of **1** in an argon-saturated aqueous nanocrystal suspension.

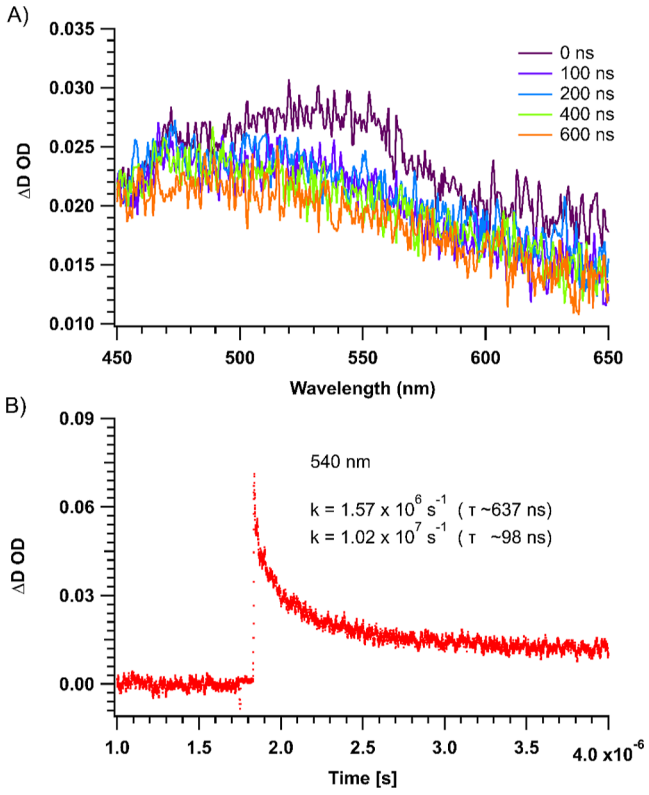

Figure 5. (A) Transient absorption spectra and (B) kinetic trace at 540 nm obtained by diffuse reflectance laser flash photolysis of **1**.

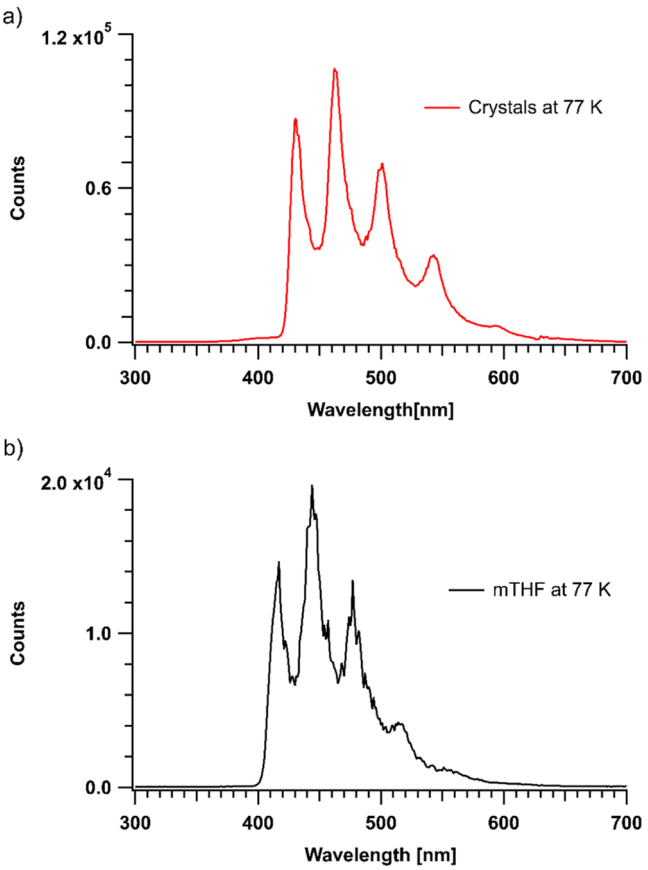

Figure 6. Phosphorescence of **1** in the (a) solid state and (b) mTHF solution at 77 K.

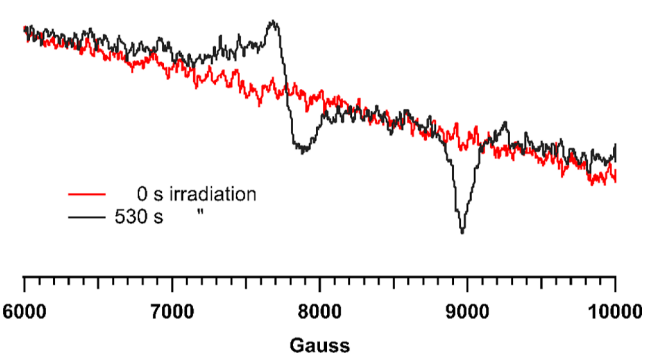

Figure 7. ESR spectra of **1** at 5 K before and after irradiation with 254 nm UV light for 530 s.

transition state barrier for T_A of **1** to form ^{3}**1N** is only ~0.25 kcal/mol, nitrene formation is efficient. In comparison, the transition state barrier for ^{3}**1N** cleavage to form the radical pair **8** and **9** is 16 kcal/mol. This energy is on the same order, within calculated uncertainty, as the energy gap between the singlet and triplet configurations of nitrene **1N**. Thus, we theorize that in the crystalline environment, nitrene ^{3}**1N** can undergo two competing reactions: intersystem crossing to ^{1}**1N** and cleavage to form the radical pair **8** and **9**. Photoproducts **3** and **5**, with the oxazolone chromophore, are formed by the insertion of ^{1}**1N** into the adjacent phenyl ring, whereas the phenol moiety originates from the cleavage of ^{3}**1N**.

We calculated a transition state barrier of 7 kcal/mol for the abstraction of an H-atom from water by radical **8**, whereas the calculated transition state barrier for **8** abstracting an H atom

https://doi.org/10.1021/acs.jpca.3c04867
J. Phys. Chem. A 2023, 127, 9705−9716

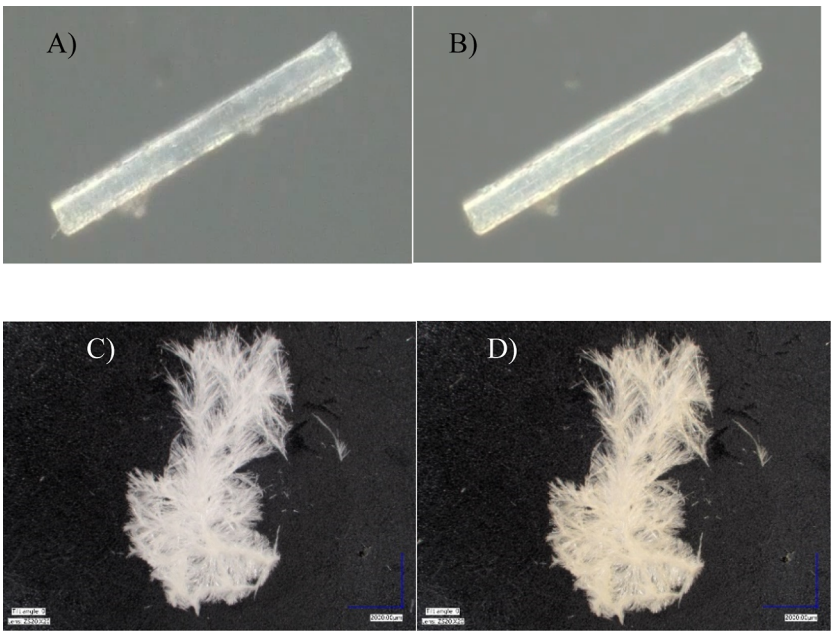

Figure 8. (A) Crystal of **1** (120 × 10 μm) grown from water and acetone; (B) after irradiating the crystal shown in (A) with a mercury arc lamp through a Pyrex filter for 19 h. (C) Crystals of **1** grown from methanol; (D) after irradiating the crystals shown in (C) with a 254 nm UV pen for **1** h.

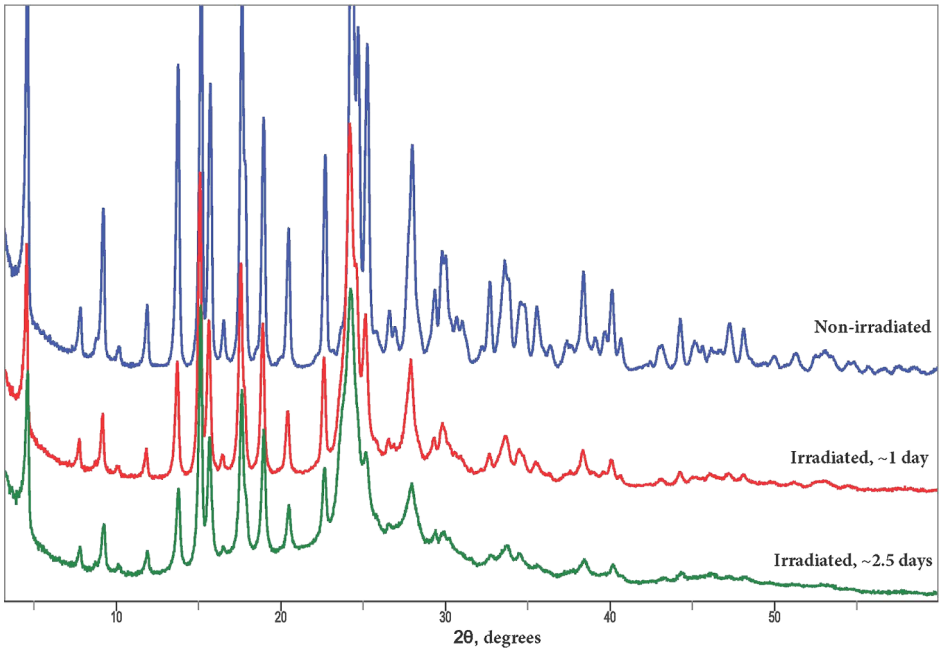

Figure 9. PXRD of **1** before and after irradiation for ~1 or ~2.5 days with a mercury arc lamp through a Pyrex filter.

from methanol is negligible. These processes are feasible at ambient temperature, which supports the notion that the H-atom source for isocyanic acid formation is atmospheric water. The transition state barrier for H atom abstraction by ^{3}**1N** from methanol is similar (8 kcal/mol) for the first H atom and ~1 kcal/mol for the second H atom. These values are comparable to those calculated previously for a methoxy carbonyl nitrene abstracting H atoms from methanol,[55] demonstrating that alkoxy nitrenes decay efficiently by H-atom abstraction and therefore have the potential for use in the light-mediated reduction of organic azides.[56] In contrast, the calculated transition state barrier for ^{3}**1N** abstracting an H atom from water is significantly larger or 18 kcal/mol, which explains why ^{3}**1N** does not decay by forming amine **2** in the solid state. Finally, the calculated transition state for phenoxy radical **9** abstracting an H atom from water is 7 kcal/mol but 13 kcal/mol for abstracting an H atom from methanol, thus water is the favored H atom source energetically. This process is feasible at ambient temperature, which supports the notion that the H-atom source for isocyanic acid formation is atmospheric water, which we cannot eliminate from the experimental procedure.

https://doi.org/10.1021/acs.jpca.3c04867
J. Phys. Chem. A 2023, 127, 9705−9716

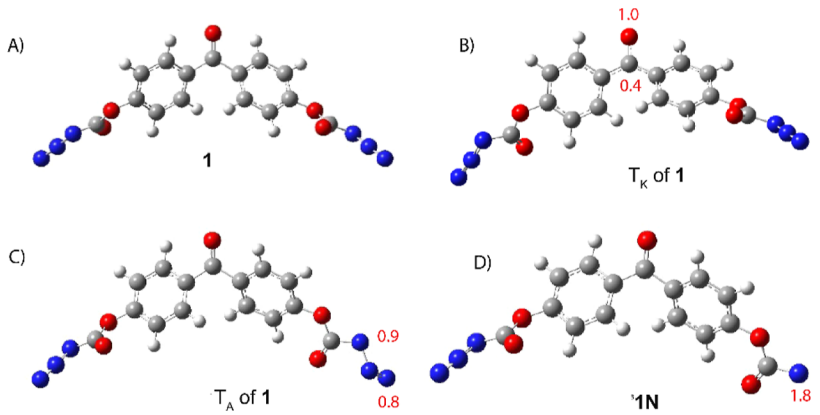

Figure 10. Optimized structures of (A) **1**, (B) T_K of **1**, (C) T_A of **1**, and (D) nitrene ^{3}**1N**. Calculated spin densities are shown with red text.

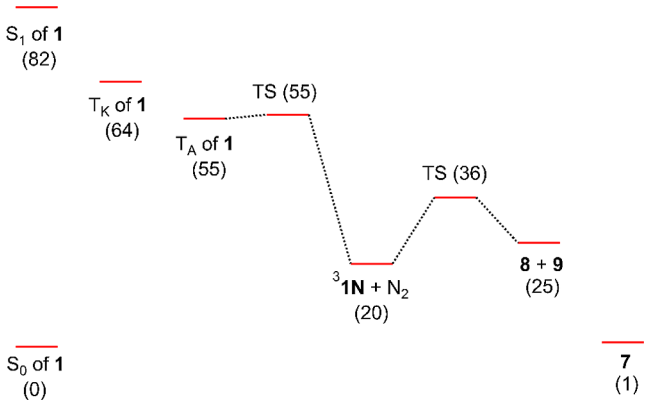

Figure 11. Calculated stationary points on the singlet and triplet surfaces of **1** [B3LYP/6-31+G(d)]. Energies are given in kcal/mol.

4. CONCLUSIONS

Irradiation of **1** in solution and the solid state leads to the formation of nitrene ^{3}**1N** through intramolecular sensitization, as confirmed by laser flash photolysis and ESR spectroscopy. In methanol, ^{3}**1N** decays by H-atom abstraction. However, in the solid state, ^{3}**1N** cleavage to form the radical pair **8** and **9** competes with intersystem crossing to its singlet configuration. Subsequently, ^{1}**1N** inserts into the adjacent phenyl ring, whereas the radical pair **8** and **9** decay by H atom abstraction to form isocyanic acid and phenol derivatives. Thus, the solid-state reactivity of **1** unmasks a reaction that is too slow to be observed in methanol. Importantly, laser flash photolysis of nanocrystals and diffuse reflectance laser flash photolysis are efficient in detecting the excited state T_K of **1** and reactive intermediate ^{3}**1N** within the crystal lattice, thus allowing elucidation of the solid-state reaction mechanism.

■ ASSOCIATED CONTENT

Supporting Information

The Supporting Information is available free of charge at https://pubs.acs.org/doi/10.1021/acs.jpca.3c04867.

IR, NMR, and HRMS of **1**−**6**; cartesian coordinates; energies; vibrational frequencies of **1**−**9**; and DLS data (PDF)

■ AUTHOR INFORMATION

Corresponding Author

Anna D. Gudmundsdottir − *Department of Chemistry, University of Cincinnati, Cincinnati, Ohio 45221-0172, United States;* orcid.org/0000-0002-5420-4098; Email: anna.gudmundsdottir@uc.edu

Authors

Noha Ahmed − *Department of Chemistry, University of Cincinnati, Cincinnati, Ohio 45221-0172, United States*

Janaka P. K. Kavikarage − *Department of Chemistry, University of Cincinnati, Cincinnati, Ohio 45221-0172, United States*

DeAnte F. Judkins − *Department of Chemistry, University of Cincinnati, Cincinnati, Ohio 45221-0172, United States*

W. Dinindu Mendis − *Department of Chemistry, University of Cincinnati, Cincinnati, Ohio 45221-0172, United States*

Rajkumar Merugu − *Department of Chemistry, University of Cincinnati, Cincinnati, Ohio 45221-0172, United States*

Jeanette A. Krause − *Department of Chemistry, University of Cincinnati, Cincinnati, Ohio 45221-0172, United States*

Bruce S. Ault − *Department of Chemistry, University of Cincinnati, Cincinnati, Ohio 45221-0172, United States;* orcid.org/0000-0003-3355-1960

Complete contact information is available at: https://pubs.acs.org/10.1021/acs.jpca.3c04867

Author Contributions

†D.F.J., W.D.M., and R.M. contributed equally.

Notes

The authors declare no competing financial interest.

■ ACKNOWLEDGMENTS

The authors thank the National Science Foundation (CHE-2102248) and the OSC (PES0597) for their generous support. WDM is grateful for a Doctoral Enhancement Fellowship from the Department of Chemistry at the University of Cincinnati. We thank Dr. McCarrick at Miami University with obtaining ESR spectra. Funding from the University of Cincinnati is acknowledged for the Rigaku MiniFlex 6G powder diffractometer.

■ REFERENCES

(1) Schmidt, G. M. J. Photodimerization in the Solid State. *Pure Appl. Chem.* **1971**, *27*, 647−678.

(2) Ramamurthy, V.; Venkatesan, K. Photochemical Reactions of Organic Crystals. *Chem. Rev.* **1987**, *87*, 433−481.
(3) Ariel, S.; Askari, S.; Evans, S. V.; Hwang, C.; Jay, J.; Scheffer, J. R.; Trotter, J.; Walsh, L.; Wong, Y.-F. Reaction Selectivity in Solid State Photochemistry. *Tetrahedron* **1987**, *43*, 1253−1272.
(4) Cohen, M. D. The Photochemistry of Organic Solids. *Angew. Chem., Int. Ed. Engl.* **1975**, *14*, 386−393.
(5) Gawande, M. B.; Bonifácio, V. D. B.; Luque, R.; Branco, P. S.; Varma, R. S. Benign by Design: Catalyst-Free in-Water, on-Water Green Chemical Methodologies in Organic Synthesis. *Chem. Soc. Rev.* **2013**, *42*, 5522−5551.
(6) Anastas, P. T.; Warner, J. C. *Green Chemistry: Theory and Practice*; Oxford University Press: Oxford, 1998.
(7) Natarajan, A.; Ng, D.; Yang, Z.; Garcia-Garibay, M. A. Parallel Syntheses of (+)- and (−)-α-Cuparenone by Radical Combination in Crystalline Solids. *Angew. Chem., Int. Ed.* **2007**, *46*, 6485−6487.
(8) Ng, D.; Yang, Z.; Garcia-Garibay, M. A. Total Synthesis of (±)-Herbertenolide by Stereospecific Formation of Vicinal Quaternary Centers in a Crystalline Ketone. *Org. Lett.* **2004**, *6*, 645−647.
(9) Mortko, C. J.; Garcia-Garibay, M. A. Green Chemistry Strategies Using Crystal-to-Crystal Photoreactions: Stereoselective Synthesis and Decarbonylation of trans-α,α'-Dialkenoylcyclohexanones. *J. Am. Chem. Soc.* **2005**, *127*, 7994−7995.
(10) Cole, J. M.; Irie, M. Solid-State Photochemistry. *CrystEngComm* **2016**, *18*, 7175−7179.
(11) Luo, J.; Ihmels, H.; Deiseroth, H.-J.; Schlosser, M. Controlling the Regioselectivity of the Di-π-Methane Rearrangements of 1,2-Naphtho-Annelated Barrelene Derivatives — Solution versus Solid-State Photochemistry. *Can. J. Chem.* **2009**, *87*, 619−626.
(12) Zimmerman, H. E.; Sereda, G. A. Solution and Crystal Lattice Effects on the Photochemistry of 6-Substituted Cyclohexenones. *J. Org. Chem.* **2003**, *68*, 283−292.
(13) Sasaki, A.; Mahé, L.; Izuoka, A.; Sugawara, T. Chemical Consequences of Arylnitrenes in the Crystalline Environment. *Bull. Chem. Soc. Jpn.* **1998**, *71*, 1259−1275.
(14) Chin, K. K.; Natarajan, A.; Gard, M. N.; Campos, L. M.; Shepherd, H.; Johansson, E.; Garcia-Garibay, M. A. Pump-Probe Spectroscopy and Circular Dichroism of Nanocrystalline Benzophenone Towards Absolute Kinetic Measurements in Solid State Photochemical Reactions. *Chem. Commun.* **2007**, 4266−4268.
(15) Kuzmanich, G.; Simoncelli, S.; Gard, M. N.; Spänig, F.; Henderson, B. L.; Guldi, D. M.; Garcia-Garibay, M. A. Excited State Kinetics in Crystalline Solids: Self-Quenching in Nanocrystals of 4,4'-Disubstituted Benzophenone Triplets Occurs by a Reductive Quenching Mechanism. *J. Am. Chem. Soc.* **2011**, *133*, 17296−17306.
(16) Shields, D. J.; Chakraborty, M.; Abdelaziz, N.; Duley, A.; Gudmundsdottir, A. D. Review of Laser Flash Photolysis of Organic Molecules (2015−2018). *Photochemistry* **2019**, *47*, 70−121.
(17) Kasai, H.; Nalwa, H. S.; Oikawa, H.; Okada, S.; Matsuda, H.; Minami, N.; Kakuta, A.; Ono, K.; Mukoh, A.; Nakanishi, H. N. H. A Novel Preparation Method of Organic Microcrystals. *Jpn. J. Appl. Phys.* **1992**, *31*, L1132−L1134.
(18) Simoncelli, S.; Kuzmanich, G.; Gard, M. N.; Garcia-Garibay, M. A. Photochemical Reaction Mechanisms and Kinetics with Molecular Nanocrystals: Surface Quenching of Triplet Benzophenone Nanocrystals. *J. Phys. Org. Chem.* **2010**, *23*, 376−381.
(19) Breslin, V. M.; Barbour, N. A.; Dang, D.-K.; Lopez, S. A.; Garcia-Garibay, M. A. Nanosecond Laser Flash Photolysis of a 6-Nitroindolinospiropyran in Solution and in Nanocrystalline Suspension under Single Excitation Conditions. *Photochem. Photobiol. Sci.* **2018**, *17*, 741−749.
(20) Naumov, P.; Karothu, D. P.; Ahmed, E.; Catalano, L.; Commins, P.; Halabi, J. M.; Al-Handawi, M. B.; Li, L. The Rise of the Dynamic Crystals. *J. Am. Chem. Soc.* **2020**, *142*, 13256−13272.
(21) Naumov, P.; Chizhik, S.; Panda, M. K.; Nath, N. K.; Boldyreva, E. Mechanically Responsive Molecular Crystals. *Chem. Rev.* **2015**, *115*, 12440−12490.
(22) Murthy, R. S.; Muthukrishnan, S.; Rajam, S.; Mandel, S. M.; Ault, B. S.; Gudmundsdottir, A. D. Triplet-Sensitized Photolysis of Alkoxycarbonyl Azides in Solution and Matrices. *J. Photochem. Photobiol., A* **2009**, *201*, 157−167.
(23) Magano, J.; Chen, M. H.; Clark, J. D.; Nussbaumer, T. 2-(Diethylamino)ethanethiol, a New Reagent for the Odorless Deprotection of Aromatic Methyl Ethers. *J. Org. Chem.* **2006**, *71*, 7103−7105.
(24) Muthukrishnan, S.; Sankaranarayanan, J.; Klima, R. F.; Pace, T. C. S.; Bohne, C.; Gudmundsdottir, A. D. Intramolecular H-Atom Abstraction in γ-Azido-Butyrophenones: Formation of 1,5 Ketyl Iminyl Radicals. *Org. Lett.* **2009**, *11*, 2345−2348.
(25) Sarkar, S. K.; Ranaweera, R. A. A. U.; Merugu, R.; Abdelaziz, N. M.; Robinson, J.; Day, H. A.; Krause, J. A.; Gudmundsdottir, A. D. Comparison of the Photochemistry of Acyclic and Cyclic 4-(4-Methoxy-phenyl)-4-oxo-but-2-enoate Ester Derivatives. *J. Phys. Chem. A* **2020**, *124*, 7346−7354.
(26) Chung, T. S.; Ayitou, A. J.-L.; Park, J. H.; Breslin, V. M.; Garcia-Garibay, M. A. *J. Phys. Chem. Lett.* **2017**, *8*, 1845−1856.
(27) Ranaweera, R. A. A. U.; Scott, T.; Li, Q.; Rajam, S.; Duncan, A.; Li, R.; Evans, A.; Bohne, C.; Toscano, J. P.; Ault, B. S.; et al. Trans-Cis Isomerization of Vinylketones through Triplet 1,2-Biradicals. *J. Phys. Chem. A* **2014**, *118*, 10433−10447.
(28) Ault, B. S. Infrared Spectra of Argon Matrix-Isolated Alkali Halide Salt/Water Complexes. *J. Am. Chem. Soc.* **1978**, *100*, 2426−2433.
(29) Frisch, M. J.; Trucks, G. W.; Schlegel, H. B.; Scuseria, G. E.; Robb, M. A.; Cheeseman, J. R.; Scalmani, G.; Barone, V.; Petersson, G. A.; Nakatsuji, H. et al. *Gaussian 16*, Revision C.01;Gaussian, Inc.: Wallingford, CT, 2016.
(30) Becke, A. D. Density-Functional Thermochemistry. III. The Role of Exact Exchange. *J. Chem. Phys.* **1993**, *98*, 5648−5652.
(31) Lee, C.; Yang, W.; Parr, R. G. Development of the Colle-Salvetti Correlation-Energy Formula into a Functional of the Electron Density. *Phys. Rev. B: Condens. Matter Mater. Phys.* **1988**, *37*, 785−789.
(32) Casida, M. E.; Jamorski, C.; Casida, K. C.; Salahub, D. R. Molecular Excitation Energies to High-Lying Bound States from Time-Dependent Density-Functional Response Theory: Characterization and Correction of the Time-Dependent Local Density Approximation Ionization Threshold. *J. Chem. Phys.* **1998**, *108*, 4439−4449.
(33) Gonzalez, C.; Schlegel, H. B. Reaction Path Following in Mass-Weighted Internal Coordinates. *J. Phys. Chem.* **1990**, *94*, 5523−5527.
(34) Gonzalez, C.; Schlegel, H. B. An Improved Algorithm for Reaction Path Following. *J. Chem. Phys.* **1989**, *90*, 2154−2161.
(35) Sigman, M. E.; Autrey, T.; Schuster, G. B. Aroylnitrenes with Singlet Ground States: Photochemistry of Acetyl-Substituted Aroyl and Aryloxycarbonyl Azides. *J. Am. Chem. Soc.* **1988**, *110*, 4297−4305.
(36) Lwowski, W.; DeMauriac, R.; Mattingly, T. W.; Scheiffele, E. Curtius-Rearrangement of "Rigid" Azides. *Tetrahedron Lett.* **1964**, *5*, 3285−3288.
(37) Wan, H.; Xu, J.; Liu, Q.; Li, H.; Lu, Y.; Abe, M.; Zeng, X. Contrasting Photolytic and Thermal Decomposition of Phenyl Azidoformate: The Curtius Rearrangement versus Intramolecular C-H Amination. *J. Phys. Chem. A* **2017**, *121*, 8604−8613.
(38) Curtius, T. 20. Hydrazide und Azide Organischer Sauren I. Abhandlung. *J. Prakt. Chem.* **1894**, *50*, 275−294.
(39) Crowley, J. N.; Sodeau, J. R. Reaction between hydrocyanic acid and O(1D2) or O(3P) oxygen atoms in low-temperature matrixes $^1D_2$) or O(^{3}P) Oxygen Atoms in Low-Temperature Matrices. *J. Phys. Chem.* **1989**, *93*, 3100−3103.
(40) Himmel, H.-J.; Junker, M.; Schnöckel, H. On the Reactivity of NH Formed from Photoinduced Decomposition of HN_3 in an Ar Matrix at 12 K toward N_2 and CO: A Combined Matrix Isolation and Quantum Chemical Study. *J. Chem. Phys.* **2002**, *117*, 3321−3326.
(41) Foresman, J. B.; Frish, C. *Exploring Chemistry with Electronic Structure Methods*; Gaussian Inc.: Pittsburgh PA, 1996.
(42) Wilkinson, F.; Kelly, G. Diffuse Reflectance Flash Photolysis. In *Handbook of Organic Photochemistry*; Scaiano, J. C., Ed.; CRC Press: Boca Raton, FL, 1989, pp 293−314.

https://doi.org/10.1021/acs.jpca.3c04867
J. Phys. Chem. A 2023, 127, 9705−9716

(43) Clark, W. D. K.; Steel, C. Photochemistry of 2,3-Diazabicyclo[2.2.2]oct-2-ene. *J. Am. Chem. Soc.* **1971**, *93*, 6347−6355.
(44) Buron, C.; Platz, M. S. Laser Flash Photolysis Study of Carboethoxynitrene. *Org. Lett.* **2003**, *5*, 3383−3385.
(45) McGlynn, S. P.; Azumi, T.; Kinoshita, M. *Molecular Spectroscopy of the Triplet State*; Prentice-Hall: Englewood Cliffs, NJ, 1969.
(46) Jin, M.; Yamamoto, S.; Seki, T.; Ito, H.; Garcia-Garibay, M. A. Anisotropic Thermal Expansion as the Source of Macroscopic and Molecular Scale Motion in Phosphorescent Amphidynamic Crystals. *Angew. Chem. Int. Ed.* **2019**, *50*, 1433−7851.
(47) Wagner, P. J.; Hammond, G. S. *Advances in Photochemistry*; Noyes, W. A., Jr.; Hammond, G. S.; Pitts, J. N., Jr., Eds.; Interscience Publishers: New York, 1968; Vol.5, pp21−156.
(48) Wasserman, E.; Snyder, L. C.; Yager, W. A. ESR of the Triplet States of Randomly Oriented Molecules. *J. Chem. Phys.* **1964**, *41*, 1763−1772.
(49) Kvaskoff, D.; Bednarek, P.; George, L.; Waich, K.; Wentrup, C. Nitrenes, Diradicals, and Ylides. Ring Expansion and Ring Opening in 2-Quinazolylnitrenes. *J. Org. Chem.* **2006**, *71*, 4049−4058.
(50) Wentrup, C. Flash Vacuum Pyrolysis of Azides, Triazoles, and Tetrazoles. *Chem. Rev.* **2017**, *117*, 4562−4623.
(51) Wentrup, C.; Kvaskoff, D. 1, 5-(1,7)-Biradicals and Nitrenes Formed by Ring Opening of Hetarylnitrenes. *Aust. J. Chem.* **2013**, *66*, 286−296.
(52) Shields, D. J.; Karothu, D. P.; Sambath, K.; Ranaweera, R. A. A. U.; Schramm, S.; Duncan, A.; Duncan, B.; Krause, J. A.; Gudmundsdottir, A. D.; Naumov, P. Cracking under Internal Pressure: Photodynamic Behavior of Vinyl Azide Crystals through N_2 Release. *J. Am. Chem. Soc.* **2020**, *142*, 18565−18575.
(53) Awad, W. M.; Davies, D. W.; Kitagawa, D.; Halabi, J. M.; Al-Handawi, M. B.; Tahir, I.; Tong, F.; Campillo-Alvarado, G.; Shtukenberg, A. G.; Alkhidir, T.; et al. Mechanical Properties and Peculiarities of Molecular Crystals. *Chem. Soc. Rev.* **2023**, *52*, 3098−3169.
(54) Sarkar, S. K.; Osisoma, O.; Karney, W. L.; Abe, M.; Gudmundsdottir, A. D. Using Molecular Architecture to Control the Reactivity of Triplet Vinylnitrene. *J. Am. Soc.* **2016**, *I*, 14905−14194.
(55) Sankaranarayanan, J.; Rajam, S.; Hadad, C. M.; Gudmundsdottir, A. D. The Ability of Triplet Nitrenes to Abstract Hydrogen Atoms. *J. Phys. Org. Chem.* **2010**, *23*, 370−375.
(56) George, S.; Govorov, D.; Gatlin, D. M.; Merugu, R.; Wasson, F. J.; Shields, D. J.; Allen, Y.; Muthukrishnan, S.; Krause, J. A.; Abe, M.; et al. Light-Mediated Synthesis of 2-(4-Methoxyphenyl)-1-pyrroline via Intramolecular Reductive Cyclization of a Triplet Alkylnitrene. *Org. Lett.* **2023**, *25*, 4345−4349.

https://doi.org/10.1021/acs.jpca.3c04867
J. Phys. Chem. A 2023, 127, 9705−9716